MOEM

Modern Electronic Materials 2020; 6(1): 31–36
DOI 10.3897/j.moem.6.1.55165

Research Article

IR luminescence of $CaGa_2O_4 : Yb^{3+}$ excited by 940 and 980 nm radiation

Ul´ana A. Mar´ina[1], Viktor A. Vorob´ev[1], Alexandr P. Mar´in[1]

1 *North-Caucasus Federal University, 1 Pushkin Str., Stavropol 355017, Russia*

Corresponding author: Ul'ana A. Mar'ina (ulyana-ne@mail.ru)

Received 12 February 2020 ♦ **Accepted** 5 March 2020 ♦ **Published** 30 March 2020

Citation: Mar′ina UA, Vorob′ev VA, Mar′in AP (2020) IR luminescence of $CaGa_2O_4 : Yb^{3+}$ excited by 940 and 980 nm radiation. Modern Electronic Materials 6(1): 31–36. https://doi.org/10.3897/j.moem.6.1.55165

Abstract

Existing calcium gallate $CaGa_2O_4$ based luminescent materials radiating in visible IR region have been reviewed. IR luminophores have been studied but slightly but their practical implementation is of interest. $CaGa_2O_4$ specimens activated with Yb^{3+} rare-earth ions have been synthesized using the solid-state method. The structure and luminescent properties of $CaGa_2O_4 : Yb^{3+}$ have been studied. $CaGa_2O_4 : Yb^{3+}$ excitation with 940 and 980 nm radiation generates luminescence in the 980–1100 nm region. Data on the electron level structure in Yb^{3+} ions suggest that the excitation and luminescence occur directly in the Yb^{3+} ions with only a passive role of the base lattice. The luminescence spectra contain three peaks at 993, 1025 and 1080 nm. These luminescence peaks are caused by electron optical transitions from excited to main state in Yb^{3+} ions. 993 nm band luminescence intensity has been studied as a function of Yb^{3+} activator ions concentration. Introduction of Na^+ ions into the luminophore increases IR luminescence intensity. Optimum $(Ca_{1-x-y}Yb_xNa_y)Ga_2O_4$ luminophore composition has been suggested at which the 993 nm luminescence intensity is the highest.

Keywords

luminophores, gallates, $CaGa_2O_4$, rare-earth elements, Yb^{3+}.

1. Introduction

The optical properties of gallates have been studied since long; particular attention is drawn by the effect of photoconductivity induced by UV excitation of the materials. Yttrium, lead, gadolinium, lithium, zinc, copper, lanthanum, barium and strontium gallates are known the photoconductivity [1, 2] and luminescent properties of which are of research interest [3–5]. However calcium gallate $CaGa_2O_4$ has been studied insufficiently in spite of its optical transparency in the visible region, high photoelectric stability and low price. On the other hand the wide band gap of $CaGa_2O_4$ (3.6 eV) and phonon oscillation frequencies in the 500–600 cm^{-1} range [3] make this material quite promising for the synthesis of new luminophores. There have been few if any studies of the luminescent properties of calcium gallate. Most of them [3, 8, 9, 11, 12] have dealt with the luminescence and electroluminescence of these materials in the visible spectral region under UV excitation.

$CaGa_2O_4$ based compounds have high chemical stability and the structure and optical properties of $CaGa_2O_4$ allow their use as an efficient luminophore matrix. These compounds have also been claimed as promising materials for electroluminescent color displays [6, 7].

Intrinsic luminescence of $CaGa_2O_4$ at λ from 300 to 600 nm and impurity $CaGa_2O_4 : Eu^{3+}, Na^+$ luminescence bands at 588 and 612 nm generated by UV excitation at λ = 255 nm were described earlier [3]. It was found [3]

that the luminophore base efficiently transfers its energy to Eu^{3+} ions and addition of Na^+ ions greatly increases the intensity and duration of the impurity luminescence. Similar conclusions were also made elsewhere [8] where red luminescence (517 nm) was observed in $CaGa_2O_4$ activated with Eu^{3+} trivalent ions. Known are the yellow $CaGa_2O_4$ based luminophores activated with Bi^{3+} [9], Mn^{2+} and Dy^{3+} ions [10] as well as the green $CaGa_2O_4$: Tb luminophore [11, 12].

Unlike visible region luminophores infrared (IR) $CaGa_2O_4$ based ones have been less studied.

It was reported [13] that $CaGa_{1.99}Cr_{0.01}O_4$ gallate has a well-developed system of traps. UV excitation causes charge accumulation and storage in deep traps. UV stimulation of traps generates wide-band Cr^{3+} radiation in the red and IR regions resembling anti-Stokes luminescence in lanthanides.

Co-activation with Cr^{3+} and Nd^{3+} ions [14] causes energy transfer from Cr^{3+} ions to Nd^{3+} ones resulting in a growth of the luminescence band at 1064 nm pertaining to Nd^{3+} ions [15]. It was suggested [14] to use these luminophores in advanced multifunctional applications for bio imaging.

Of interest is also a study [16] of Stokes $CaGa_2O_4$ based luminophores activated with Nd^{3+} ions and different sensibilizers (Bi^{3+}, Eu^{3+}, Cr^{3+}) where the possibility of near-UV transformation of blue exciting radiation into near-IR region radiation was investigated. These processes are based on energy accumulation and transfer from sensibilizing ions to Nd^{3+} ions. Cr^{3+} ions have a broad excitation spectrum in the blue UV region and as reported earlier [16] most efficiently transfer energy to Nd^{3+} ions which in turn generate IR luminescence at ~1000 nm [16]. This material was suggested as a promising spectral converter for silicon solar cells.

The $CaGa_2O_4$: Yb^{3+} excitation spectra [16] contained two bands: a wide one at λ = 200–255 nm corresponding to interband transitions in the $CaGa_2O_4$ base lattice and a peak series at 900–1000 nm caused by transitions in Nd^{3+} ions. Luminescence in Eu^{3+},Yb^{3+} : $CaGa_2O_4$, Bi^{3+},Yb^{3+} : $CaGa_2O_4$, Cr^{3+},Yb^{3+} : $CaGa_2O_4$ compounds was excited with 266 and 450 nm sources. Luminescence was excited through the luminophore base and sensibilizing impurity. $CaGa_2O_4$: Yb^{3+} luminescence excitation with 900–1000 nm radiation was not studied [16]. However IR-excited IR luminophores are also of research interest and can be used for the fabrication of spectral photoconverters, latent images and markers.

Presented below are data on the luminescent properties of $CaGa_2O_4$ activated with Yb^{3+}ions upon 940 and 980 nm laser excitation.

2. Experimental

The raw materials for luminophore synthesis were special purity $CaCO_3$ calcium carbonate, Ga_2O_3 gallium oxide, Yb_2O_3 ytterbium oxide and Na_2CO_3 sodium carbonate. Due to the small required quantity of rare-earth Nd^{3+} ions they were introduced into the charge in the form of $Yb(NO_3)_3$ nitrate in concentrations of 0.3 to 15 mol.%. Along with the activator ions, charge compensating Na^+ ions were introduced into the luminophore. Their concentration was the same as that of Nd^{3+} ions. The empirical formula of the synthesized luminophore was $(Ca_{1-x-y}Yb_xNa_y)Ga_2O_4$. The luminophore was synthesized using the solid-state method in a high-temperature furnace in an air atmosphere at 1250 °C for 18 h. These temperature and time parameters were selected based on experimental X-ray diffraction data on specimens synthesized under different conditions. Detailed description of α-$CaGa_2O_4$ and β-$CaGa_2O_4$ polymorphic phase formation in the 1050–1350 °C range was reported earlier [7]. The 1250–1350 °C range is the optimum one for synthesizing the $CaGa_2O_4$ phase at normal atmospheric pressure in the presence of oxygen gas.

In accordance with earlier data [12] three compounds may exist in the CaO–Ga_2O_3 system depending on the stoichiometric ratio: 3CaO · Ga_2O_3, CaO · Ga_2O_3 and CaO · $2Ga_2O_3$. To obtain the CaO · Ga_2O_3 phase (hereinafter $CaGa_2O_4$) we added the CaO and Ga_2O_3 components in the 1 : 1 ratio.

Qualitative and quantitative phase analyses of the specimens were carried out on the basis of X-ray diffraction patterns taken on a DIFREI 401 X-ray diffraction instrument in CuK_α radiation with a Ni filter. The unit cell parameters were calculated using the Difract software.

The size distribution of the synthesized powders was studied with a Microsizer 201A laser analyzer [17].

The excitation spectra were analyzed using two MDR-24 monochromators and a photocell device for IR radiation detection. The luminescence spectra were taken with an MDR-204 monochromator and a PbS photocell device. The luminescence was excited with 940 and 980 nm semiconductor laser diodes.

The reference specimen for the spectral analysis of the synthesized specimens was L-54 industrial luminophore. The maximum luminescence band intensity ratio in the 980–1100 nm region for the test and reference specimens was used as the IR luminescence intensity measure.

3. Results and discussion

Solid state synthesis of calcium gallate includes baking of two CaO and Ga_2O_3 oxides at 1250 °C for 18 h. The reaction formula is [18]

$$CaO + Ga_2O_3 \rightarrow CaGa_2O_4. \quad (1)$$

Calcium gallate ($CaGa_2O_4$) crystallizes predominantly in the orthorhombic modification, space group $P21/c$ [19, 20]. The ionic radius of Ca^{2+} (0.099 nm) is comparable with that of the activator ions Yb^{3+} (0.086 nm) [21, 22], the Ga^{3+} ionic radius being far smaller, 0.062 nm [12]. Therefore upon introduction of Yb^{3+} ions into $CaGa_2O_4$ structure, these activator ions most probably occupy Ca^{2+} ion positions to

form a substitutional solid solution. This however causes a charge mismatch that we compensated with Na^+ ions by introducing them into the luminophore charge in the same quantity as Yb^{3+} ions. The Na^+ ionic radius (0.097 nm) is almost the same as that of Ca^{2+}, and this is also expected to reduce structure distortion in the base lattice.

Figure 1 shows X-ray diffraction patterns of pure and Yb^{3+} and Na^+ doped calcium gallate. By way of comparison we presented the bar chart for $CaGa_2O_4$ borrowed from the ASTM international X-ray diffraction standard files, card No. PDF-140143.

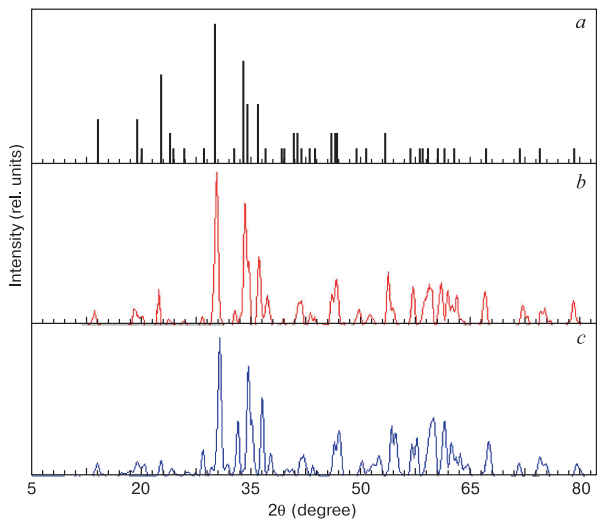

Figure 1. (*a*) Bar chart and experimental X-ray diffraction patterns of (*b*) pure $CaGa_2O_4$ and (*c*) doped $CaGa_2O_4$: Yb,Na.

The most prominent diffraction peaks in the X-ray diffraction patterns coincide with the typical peaks of $CaGa_2O_4$ (PDF-140143) as per the ASTM X-ray diffraction files. It can also be seen from Fig. 1 that the typical diffraction peaks of the pure and doped calcium gallate coincide. This is caused by the low Yb^{3+} and Na^+ doping impurity concentrations which incorporate into the gallate lattice and occupy Ca^{2+} ion positions without causing considerable distortion to the material's crystal lattice.

The size distribution of the powdered specimens synthesized under similar conditions showed that the mean particle size of pure $CaGa_2O_4$ is 17.9 µm. The mean particle size of $CaGa_2O_4$ activated with 5 mol.% Yb^{3+} ions is 18.5 µm. Introduction of Na^+ ions into the luminophore in the same quantity increases the mean particle size but slightly to 21.7 µm. This is because Na_2CO_3 impurity acts as flux during solid state luminophore synthesis thus improving the interaction between solid solution components and accelerating mass transport and new phase formation. As a result the crystallites grow and the mean particle size in the specimen increases.

The excitation spectra of the $(Ca_{0,9}Yb_{0,05}Na_{0,05})Ga_2O_4$ luminophore were taken for 1025 and 1080 nm luminescent bands which were selected based upon a preliminary study of specimen luminescence spectra excited with a 980 nm laser. The excitation wavelength used for excitation spectra measurement was varied in the 800 to 2000 nm range. The 1025 nm band in the excitation spectra corresponded to two peaks at 923 and 975 nm. For the 1080 nm band the maximum excitation intensity was at the same wavelengths (Fig. 2). The spectra also contained one more excitation band at ~910 nm but its peak was less clear.

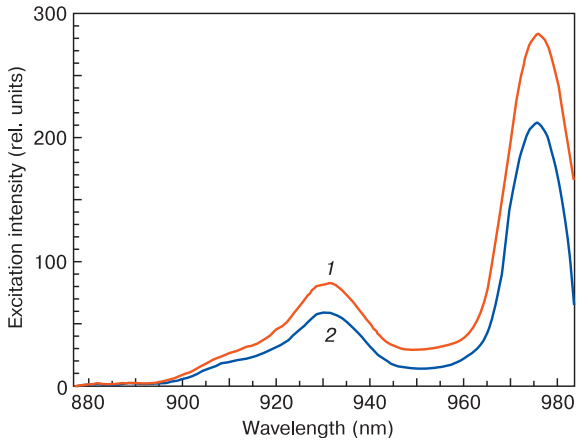

Figure 2. $(Ca_{0,9}Yb_{0,05}Na_{0,05})Ga_2O_4$ luminophore specimen excitation spectra: (*1*) 1025 and (*2*) 1080 nm.

As noted above the $CaGa_2O_4$ band gap is about 3.6 eV. To make the energy of valence electrons sufficient for electron transition to the conduction band one should excite the material with a 344 nm or smaller wavelength radiation. This may initiate interband transitions. These transitions in $CaGa_2O_4$ were described in an earlier study of intrinsic and extrinsic UV-excited visible luminescence [3, 16]. Since IR luminescence was excited in our experiment with photons having far greater wavelengths one can conclude that their energy would be insufficient for interband transitions. Thus electron transitions in $CaGa_2O_4$: Yb^{3+} occurred directly in Yb^{3+} activator ions with only a passive role of the base lattice.

Excitation at the 910, 932 and 975 nm corresponds to energy transfers between Stark components of the $^2F_{7/2}$ and $^2F_{5/2}$ levels in Yb^{3+} ions. Since the excitation intensity for the 932 and 975 nm bands was the highest we used 940 and 980 nm semiconductor laser diodes for further luminescence studies of the test specimens.

We now consider excitation and luminescence in $CaGa_2O_4$: Yb^{3+} in a greater detail using the electron level diagram of Yb^{3+} ions (Fig. 3). Data on the positions of the top Stark levels were borrowed from an earlier study of electron absorption spectra [18], and the structure of the bottom Stark sublevels of Yb^{3+} ions was studied using luminescence spectra [23, 24].

The main unexcited level $^2F_{7/2}$ consists of four Stark sublevels (1, 2, 3, 4) and the excited level $^2F_{5/2}$ is split into three sublevels (5, 6, 7). Arrows show potential electron transitions with energy absorption or release. Earlier absorption and luminescence spectra [18, 23, 24] were studied at LN or lower temperatures. This greatly reduced the

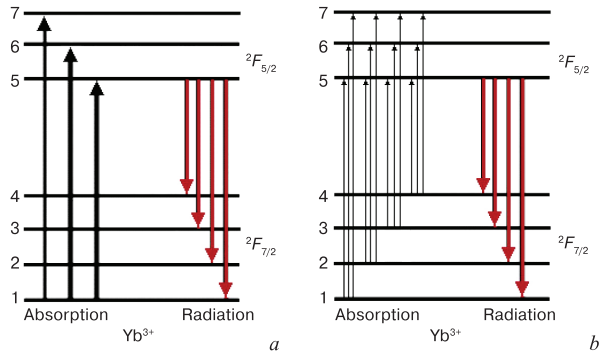

Figure 3. Structure of Stark sublevels in Yb^{3+} ions: (*a*) 4.2–77 K transitions [23, 24]; (*b*) 300 K transitions.

thermal oscillation energy of the lattice atoms for more reliable matching of absorption peaks with the respective transitions between Stark components in Yb^{3+} ions. It was reported [23] that at 4.2 K transitions may occur from the main bottom Stark sublevel $^2F_{7/2}$ (1) to the excited Stark sublevels 5, 6 and 7 of the $^2F_{5/2}$ state (Fig. 3*a*).

We studied the material at room temperature (300 K). The occupation of the Stark sublevels 2, 3 and 4 at this temperature is greater than at 4.2 K and therefore there is a higher probability of electron transitions from these levels to the $^2F_{5/2}$ multiplet sublevels (Fig. 3*b*). Electron transitions from the bottom sublevel 5 of the excited $^2F_{5/2}$ state to the sublevels 1, 2, 3 and 4 of the $^2F_{7/2}$ state is accompanied by energy release in the form of a photon, i.e., luminescence occurs. The same conclusions were made in a earlier study of the Stark structure of Yb^{3+} ion levels in $(Yb_xY_{1-x})_2Ti_2O_7$ at 4.5–300 K [25].

The first stage of our investigation into the luminescent properties of $CaGa_2O_4$: Yb^{3+} dealt with the luminescence spectra of the specimens and the effect of Na^+ ions on the luminescence intensity. The luminescence spectra of the specimens contain three resolvable peaks at 993, 1025 and 1080 nm (Fig. 4). Radiation at these wavelengths is generated by electron transitions from the excited $^2F_{5/2}$ level to the main unexcited $^2F_{7/2}$ level in Yb^{3+} ions.

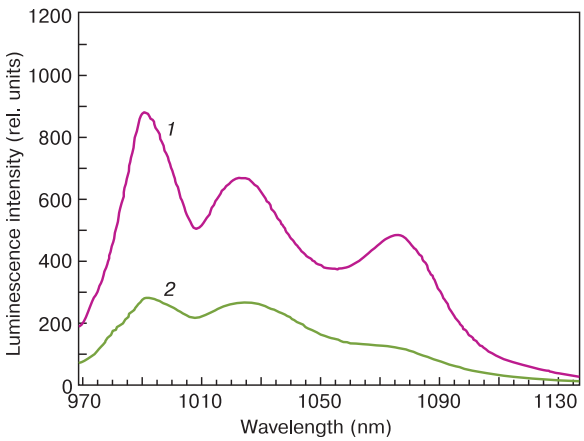

Figure 4. (*1*) $(Ca_{0.9}Yb_{0.05}Na_{0.05})Ga_2O_4$ and (*2*) $(Ca_{0.95}Yb_{0.05})Ga_2O_4$ luminescence spectra excited with 940 nm radiation.

The 993 nm luminescence intensity in the specimen synthesized with flux was almost threefold higher than that in the specimen synthesized without flux. This confirms our assumptions concerning the effect of Na^+ ions on the luminescent properties of $CaGa_2O_4$: Yb^{3+}. We will now consider in detail the process of charge compensation upon the formation of a substitutional solid solution.

Yb^{3+} ions in $CaGa_2O_4$: Yb^{3+} occupy the positions of Ca^{2+} ions. Inovalent substitution produces electrically charged defects. Two Yb^{3+} ions substitute three Ca^{2+} ions thus generating one negatively charged defect V''_{Ca} and two positively charged defects $Yb^{\bullet}_{Ca}$ the defect formation reaction being as follows:

$$3Ca^{2+} + 2Yb^{3+} \rightarrow V''_{Ca} + 2Yb^{\bullet}_{Ca}. \quad (1)$$

Ca^{2+} ion substitution for Na^+ and Yb^{3+} ions in the lattice generates one positively charged defect $Yb^{\bullet}_{Ca}$ and one negatively charged defect Na°_{Ca}. The defect formation equation is as follows:

$$2Ca^{2+} + Na^{+} + Yb^{3+} \rightarrow Na^{\circ}_{Ca} + Yb^{\bullet}_{Ca}. \quad (2)$$

It is well-known [3] that Na^+, Li^+ and K^+ ions not only act as charge compensators but also affect to a certain extent the crystal lattice, powder particle size and surface morphology of the material. The Na^+ ionic radius (0.097 nm) is almost the same as that of Ca^{2+} ions (0.099 nm) so the structural distortions caused by their mutual replacement in the $CaGa_2O_4$ lattice are but minor. Thus introduction of Na^+ ions into the luminophore minimizes the role of defects generated by violation of crystal electrical neutrality and size mismatch between Ca^{2+} and Yb^{3+} ions and hence increases the luminescence intensity in the 980–1090 nm region.

At the second stage we studied the luminescence intensity in the specimens as a function of Yb^{3+} ions concentration. Figure 5 shows luminescence spectra of $(Ca_{1-x-y}Yb_xNa_y)Ga_2O_4$ for different activator ion concentrations.

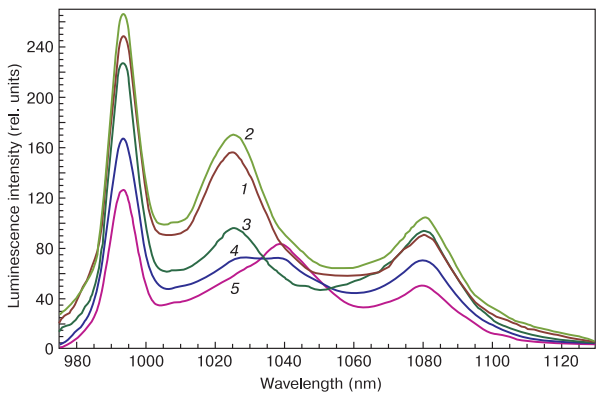

Figure 5. $(Ca_{1-x-y}Yb_xNa_y)Ga_2O_4$ luminescence spectra excited with 940 nm radiation for different activator ion concentrations: (*1*) $x = y = 0.5$ mol.%; (*2*) 1 mol.%; (*3*) 5 mol.%; (*4*) 10 mol.%; (5) 15 mol.%.

The luminescence spectrum of $(Ca_{1-x-y}Yb_xNa_y)Ga_2O_4$ is a broad band with three clearly resolved peaks at 993, 1025 and 1080 nm and a few weak peaks. The luminescence intensity is the highest for the specimen with an Yb^{3+} ions concentration of 1 mol.%. The luminescence intensity decreases with an increase in the activator ion concentration. At Yb^{3+} ions concentrations of 10 and 15 mol.% the luminescence spectrum exhibits intensity redistribution between the 1025 nm peak which is strong at low Yb^{3+} and Na^+ concentrations and the weak peaks in the vicinity of 1040 nm, in favor of the latter ones. This can be caused by structural distortions in the base lattice and new phase formation. To exclude the effect of occasional errors in the synthesis or study of the specimens we synthesized one more series of specimens with the same Yb^{3+} concentrations. The luminescence spectra of the specimens containing 10 and 15 mol.% Yb^{3+} ions exhibited a similar intensity redistribution.

Figure 6 shows 993 nm luminescence intensity as a function of Yb^{3+} ions concentration.

To obtain a more accurate concentration function we synthesized an additional series of specimens with the Yb^{3+} concentrations x = 0.003, 0.007, 0.01, 0.02 and 0.03. The highest 993 nm luminescence intensity in $(Ca_{1-x-y}Yb_xNa_y)Ga_2O_4$ was observed at the Yb^{3+} concentration x = 0.01. The optimum luminophore composition for this spectral band is $(Ca_{0.98}Yb_{0.01}Na_{0.01})Ga_2O_4$.

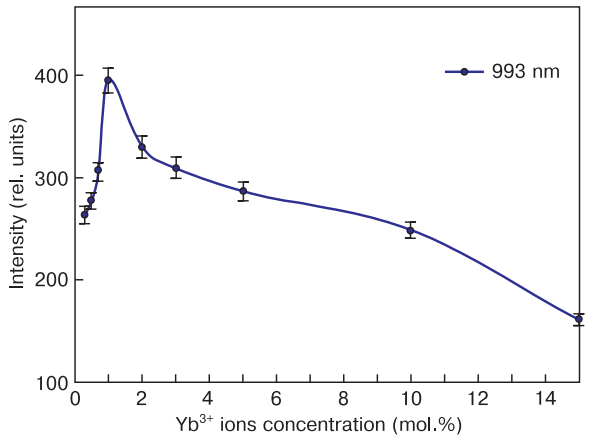

Figure 6. 993 nm luminescence band intensity of $(Ca_{1-x-y}Yb_xNa_y)Ga_2O_4$ ($x = y$ = 0.3; 0.5; 0.7; 1; 2; 3; 5; 10; 15 mol.%) as a function of Yb^{3+} ions concentration for 940 nm excitation.

4. Conclusion

Study of the $CaGa_2O_4 : Yb^{3+}$ compound showed that excitation of the material with 940 and 980 nm radiation generates luminescence in the 980–1100 nm region with peaks at 993, 1025 and 1080 nm. The luminescence in this region is caused by optical transitions in Yb^{3+} ions. Experiments prove the potential for enhancing this IR luminescence by introducing the Na_2CO_3 compensating impurity into the luminophore. Study of the luminescence intensity as a function of activator ions concentration showed that the highest 993 nm luminescence intensity is at the Yb^{3+} concentration x = 0.01. The optimum luminophore composition was suggested to be $(Ca_{0.98}Yb_{0.01}Na_{0.01})Ga_2O_4$.

The IR luminophores suggested in this work can find applications in biomedicine, laser engineering, marking expensive products and art pieces, military engineering and fiber optics.

References

1. Bletskan D.I., Kabatsii V.M., Kranichets M., Frolova V.V., Gule E.G. Photoconductivity and photoluminescence of $PbGa_2Se_4$ crystals. *Chalcogenide Letters*. 2006; 3(12): 125–132. http://www.chalcogen.ro/Bletskan-articol.pdf
2. Bordun O.M., Bihday V.G., Kukharskyy I.Yo. Influence of annealing conditions on the luminescence and photoelectric properties of pure and Mn^{2+}-activated $ZnGa_2O_4$ thin films. *J. Appl. Spectrosc*. 2013; 80(5): 721–725. https://doi.org/10.1007/s10812-013-9832-2
3. Rai M., Singh S.K., Mishra K., Shankar R., Srivastava R.K., Rai S.B. Eu^{3+}-activated $CaGa_2O_4$ wide band gap (WBG) material for solar blind UV conversion: fluorescence and photo-conductivity performance. *J. Mater. Chem. C*. 2014; 2(37): 7918–7926. https://doi.org/10.1039/C4TC00965G
4. Glasser F.P., Glasser L.S.D. Crystal chemistry of some AB_2O_4 compounds. *J. American Ceramic Society*. 1963; 46(8): 377–380. https://doi.org/10.1111/j.1151-2916.1963.tb11755.x
5. Mar′ina U.A., Vorob′ev V.A., Mar′in A.P., Pigulev R.V. Luminescent properties of strontium gallate activated by europium ions. In: Actual problems of engineering sciences: materials of the VIIth (64th) annual scientific-practical conference of teachers, students and young scientists of the North Caucasus Federal University «University Science – Region». Stavropol, 2019: 470–472. (In Russ.)
6. Patent EP 0836791 B1H05B 33/14, C09K 11/80, C09K 11/66. International publication number: WO 97/02721. Doped amorphous and crystalline gallium oxides, alkaline earth gallates and doped zinc germanate phosphors as electroluminescent materials. T. Hamilton, A.H. Hamilton, G. Edmonton, 1998.
7. Jiang F., Jiang P., Yue M., Gao W., Cong R., Yang T. Temperature-induced phase transitions for stuffed tridymites $SrGa_2O_4$ and $CaGa_2O_4$. *J. Solid State Chem*. 2017; 254: 195–199. https://doi.org/10.1016/j.jssc.2017.07.024
8. Ye D., Hu Z., Zhang W., Cui Y., Luo L., Wang Y. Inner energy transfer and its influence on luminescence properties of $CaGa_2O_4$:Eu^{3+} reddish emission phosphors. *Optical Materials*. 2014; 39(11): 1879–1882. https://doi.org/10.1016/j.optmat.2014.04.028
9. Wang S., Chen W., Zhou D., Qiu J., Xu X., Yu X. Long persistent properties of $CaGa_2O_4$:Bi^{3+} at different ambient temperature. *The American Ceramic Society*. 2017; 100(8): 3514–3521. https://doi.org/10.1111/jace.14875
10. Keir P.D. Fabrication and characterization of ACTFEL devices: Diss. of PhD. Oregon State University, 2000, 280 p.

11. Minami T. Thin-film oxide phosphors as electroluminescent materials. *Materials Research Society*. 1999; 560: 47–58. https://doi.org/10.1557/PROC-560-47
12. Jeevaratnam J., Glasser F.P. The System CaO-Ga_2O_3. *J. American Ceramic Society*. 1961; 44(11): 563–566. https://doi.org/10.1111/j.1151-2916.1961.tb11658.x
13. Rai M., Singh S. K., Morthekai P. Laser-induced excited-state crossover and spectral variation of Cr^{3+} in the high-crystal-field environment of $CaGa_2O_4$. *Opt. Lett*. 2016; 41(15): 3635–3638. https://doi.org/10.1364/OL.41.003635
14. Qin X., Li Y., Zhang R., Ren J., Gecevicius M., Wu Y., Sharafudeen K., Dong G., Zhou S., Ma Z., Qiu J. Hybrid coordination-network-engineering for bridging cascaded channels to activate long persistent phosphorescence in the second biological window. *Sci. Rep.* 2016; 6: 20275(1–9). https://doi.org/10.1038/srep20275
15. Mar′ina U.A., Vorob′ev V.A., Mar′in A.P., Pigulev R.V. Study of the luminescent properties of $SrGa_2S_4$ activated by rare-earth ions Nd^{3+} In: Physics. Technology. Innovation FTI-2019: a collection of abstracts of the VI International Youth Scientific Conference dedicated to the 70th anniversary of the founding of the Physicotechnological Institute. Yekaterinburg, 2019: 737–738. (In Russ.)
16. Rai M., Mishra K., Rai S.B., Paulramasamy M. Tailoring UV-blue sensitization effect in enhancing near infrared emission in X,Yb^{3+}:-$CaGa_2O_4$ (X = 0, Eu^{3+}, Bi^{3+}, Cr^{3+}) phosphor for solar energy conversion. *Materials Research Bulletin*. 2018; 105: 192–201. https://doi.org/10.1016/j.materresbull.2018.04.051
17. Mar′ina U.A. Development of synthesis technology and study of phosphors based on $CaSnO_3$, $BaSnO_3$, $SrSnO_3$, activated by rare-earth ions: PhD thesis. Novocherkassk, 2018: 52–58. (In Russ.)
18. Ropp R.C. Encyclopedia of the Alkaline Earth Compounds. Ch. 6: Group 13 (B, Al, Ga, In and Tl) Alkaline Earth Compounds. Elsevier, 2013: 586–587. https://doi.org/10.1016/C2012-0-00777-6
19. Akimova M.S. Phase formation and crystalline structure formation upon receipt of calcium monoaluminate and luminescent materials based on it using the sol-gel method: master's thesis. Tomsk, 2019, 35 p. (In Russ.)
20. Weber M.J. Handbook of optical materials. CRC Press, 2003, 536 p. https://doi.org/10.1201/9781420050196
21. Shannon R.D., Prewitt C.T. Effective ionic radii in oxides and fluorides. *Acta Crystallographica. Section B.* 1969; 25(5): 925–946. https://doi.org/10.1107/S0567740869003220
22. Ahrens L.H. The use of ionization potentials. Pt. 1. Ionic radii of the elements. *Geochimica et Cosmochimica Acta*. 1952; 2(3): 155–169. https://doi.org/10.1016/0016-7037(52)90004-5
23. Guzik M., Tomaszewicz E., Guyot Y., Legendziewicz J., Boulon G. Spectroscopic properties, concentration quenching and Yb^{3+} site occupations in vacancied scheelite-type molybdates. *J. Luminescence*. 2016; 169(2): 755–764. https://doi.org/10.1016/j.jlumin.2015.02.043
24. Guzik M., Bieza M., Tomaszewicz E., Guyot Y., Boulon G. Research on the Yb^{3+} ion activated cubic molybdates and molybdato-tungstates for optical transparent ceramics. In: Quantum Nano-Photonics. NATO 2017. Dordrecht: Springer, 2018; 17: 315–354. https://doi.org/10.1007/978-94-024-1544-5_17
25. Klimin S.A., Popova M.N., Chukalina E.P., Malkin B.Z., Zakirov A.R., Antic-Fidancev E., Goldner Ph., Aschehoug P., Dhalenne G. Stark structure of the Yb^{3+} ion levels in $(Yb_xY_{1-x})_2Ti_2O_7$ and the crystal field in rare-earth titanates with a pyrochlore structure. *Phys. Solid State*. 2005; 47(8): 1425–1430. https://doi.org/10.1134/1.2014481